water

MDPI

Article

Taguchi L25 (5^4) Approach for Methylene Blue Removal by Polyethylene Terephthalate Nanofiber-Multi-Walled Carbon Nanotube Composite

Wafa K. Essa [1], Suhad A. Yasin [1,*], Anwar H. Abdullah [1], Mohammad R. Thalji [2], Ibtisam A. Saeed [1], Mohammed A. Assiri [3,4], Kwok Feng Chong [5] and Gomaa A. M. Ali [6,*]

1 College of Science, University of Duhok, Duhok 42001, Iraq; wafa.k.essa@uod.ac (W.K.E.); anwar.hadi@uod.ac (A.H.A.); ibtisamsaid@uod.ac (I.A.S.)
2 Independent Researcher, Amman P.O. Box 26110, Jordan; mdthalji@gmail.com
3 Research Center for Advanced Materials Science (RCAMS), King Khalid University, P.O. Box 80203, Abha 61413, Saudi Arabia; assiri999@hotmail.com
4 Department of Chemistry, Faculty of Science, King Khalid University, P.O. Box 9004, Abha 61413, Saudi Arabia
5 Faculty of Industrial Sciences & Technology, Universiti Malaysia Pahang, Gambang, Kuantan 26300, Malaysia; ckfeng@ump.edu.my
6 Chemistry Department, Faculty of Science, Al–Azhar University, Assiut 71524, Egypt
* Correspondence: suhad.yasin@uod.ac (S.A.Y.); gomaasanad@azhar.edu.eg (G.A.M.A.)

Abstract: A membrane composed of polyethylene terephthalate nanofiber and multi-walled carbon nanotubes (PET NF-MWCNTs) composite is used to adsorb methylene blue (MB) dye from an aqueous solution. Scanning electron microscopy, Fourier transform infrared spectroscopy, and X-ray diffraction techniques are employed to study the surface properties of the adsorbent. Several parameters affecting dye adsorption (pH, MB dye initial concentration, PET NF-MWCNTs dose, and contact time) are optimized for optimal removal efficiency (R, %) by using the Taguchi L25 (5^4) Orthogonal Array approach. According to the ANOVA results, pH has the highest contributing percentage at 71.01%, suggesting it has the most significant impact on removal efficiency. The adsorbent dose is the second most affected (12.08%), followed by the MB dye initial concentration of 5.91%, and the least affected is the contact time (1.81%). In addition, experimental findings confirm that the Langmuir isotherm is well-fitted, suggesting a monolayer capping of MB dye on the PET-NF-MWCNT surface with a maximum adsorption capacity of 7.047 mg g^{-1}. Also, the kinetic results are well-suited to the pseudo-second-order model. There is a good agreement between the calculated (q_e) and experimental values for the pseudo-second-order kinetic model.

Keywords: taguchi approach; ANOVA; nanofibers; methylene blue; adsorption; removal efficiency; multi-walled carbon nanotubes

Citation: Essa, W.K.; Yasin, S.A.; Abdullah, A.H.; Thalji, M.R.; Saeed, I.A.; Assiri, M.A.; Chong, K.F.; Ali, G.A.M. Taguchi L25 (5^4) Approach for Methylene Blue Removal by Polyethylene Terephthalate Nanofiber-Multi-Walled Carbon Nanotube Composite. *Water* **2022**, *14*, 1242. https://doi.org/10.3390/w14081242

Academic Editor: Ahmed Abou-Shady

Received: 11 March 2022
Accepted: 6 April 2022
Published: 12 April 2022

1. Introduction

Chemical and biological effluents from industrial processes contribute to environmental pollution and resource depletion [1]. Industrial dyes, for example, are widely used in a diverse range of industries, including textiles and the food industry. Furthermore, they are utilized in cosmetics and paintings, and they are released into the environment regularly. Based on current estimates, between 10% and 15% of the 0.8 million tons of dyes generated yearly around the globe are harmful to the environment and human health [2]. One of the most commonly used dyes in the medical, chemical, and biological fields is methylene blue (MB), a cationic dye [3]. When humans or animals consume MB dye, they may notice complications such as eye burns, rapid breathing, nausea, and vomiting. Unfortunately, it has been reported that various symptoms may manifest themselves in both humans and animals when MB dye accumulates in wastewater [4,5].

As a result, several physicochemical and biological wastewater treatment strategies have been effectively adopted [6]. Membrane filtration [7], photodegradation [8–12], irradiation [13], biological treatment [14], adsorption [15–19], and ultrasonic-assisted adsorption [20] are all strategies for wastewater recovery. Adsorption is still the most common way to get rid of contaminants from aquatic environments [18,21–23] because it is simple, effective, and cheap. When considering adsorption capacity, it is critical to examine the adsorbent's physicochemical parameters and chemical composition. Particle dispersion, shape, and size are all aspects of physicochemical features. Importantly, the adsorption process is easily controllable and modelable [24,25], a significant advantage.

Different materials, such as metal-organic frameworks (MOFs) [26], nanoscale zero-valent irons (nZVI) [27], and carbon nanotubes (CNTs) [28,29], have been employed to remove various contaminants from wastewater in the past few years. CNTs are used to remove dyes from wastewater due to their high mechanical strength, low cost, and high affinity for pollutant molecules [30]. Carbon nanotubes (CNTs) can be modified via polymers to enhance their electrical, mechanical, and thermomechanical characteristics [31,32]. It was because of their high surface area, high porosity, hollow and layered structures, and electrical and hydrophobic interactions with pollutant ions. They have attracted the attention of those interested in removing dye pollutants from wastewater [33,34]. They are classified as single-walled carbon nanotubes (SWCNTs) and multi-walled carbon nanotubes (MWCNTs) [35]. The layout of graphene cylinders change between the two types of CNTs. MWCNTs are created by rolling graphene into concentric tubes (many layers) and then connecting them to form a single structure. They have higher adsorption effectiveness than SWCNTs due to their greater surface area per unit weight [36].

Nanotechnologies are vital to preventing undesirable health effects and promoting environmental protection [37] when it comes to environmentally friendly technologies such as wastewater treatment [38] and air purification techniques [39]. Electrospinning has evolved into a straightforward and dependable technology for producing polymer nanofiber membranes with wide pore sizes and a high surface area [40,41]. They have been widely employed in various applications, including tissue engineering, oil/water separation, catalysis, energy storage/conversion, and adsorption [42–45]. Furthermore, by introducing nanoparticles as additives into a polymer nanofiber membrane, the resulting nanocomposite membrane can be increased in other characteristics, such as adsorption, while demonstrating just a modest loss in membrane permeability. Different nanocomposite membrane fabrication strategies can be traced to these blended nanomaterials' enhanced surface modification capabilities. These methods may make it easier to remove ions and speed up the adsorption process [46–48].

This work aims to provide a detailed insight into how PET NF-MWCNTs composites can effectively remove the MB dye from an aqueous solution. The effects of various parameters on the adsorption of MB dye on composites are thoroughly studied. Solution pH, MB dye concentration, PET NF-MWCNTs dose, and contact time. Additionally, the isotherms, kinetics, and mechanism of the adsorption process are determined. The results show that removing MB dye from a solution using a PET NF-MWCNTs composite adsorbent is successful. The current work is shown schematically in Scheme 1.

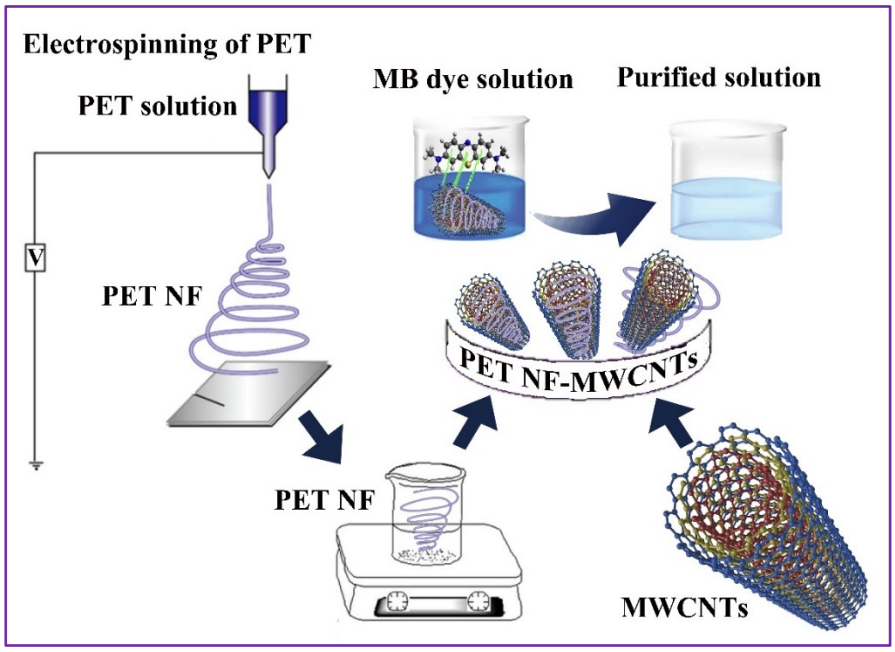

Scheme 1. The schematic representation of the current work methodology.

2. Materials and Methods

2.1. Materials

MWNTs were provided by the National and Medical Science Research Center, Nizwa, Oman [49]. MB ($C_{16}H_{18}N_3SCl.3H_2O$) dye was purchased from Sigma Aldrich, with λ_{max} of 660 nm. Sodium hydroxide (NaOH, 98%) and hydrochloric acid (HCl, 37%) were purchased from Scharlau. All chemicals were analytical grade and used immediately, without any purification.

2.2. Preparation of PET NF-MWCNTs Composite

Similar to the previous work [50], PET NF was fabricated by electrospinning. The materials were dissolved in acetone with stirring for 2 h at room temperature. The materials were dissolved in acetone with stirring for 2 h at room temperature. Factors influencing the electrospinning process were adjusted to1 mL/h, 15 cm, 5%, and 15 kV for flow rate, needle to collector distance, PET concentration, and the applied voltage, respectively. Preparing the PET NF-MWCNTs composite started with 0.185 g of PET NF, which was treated with 3.0 mL of 0.5 M NaOH and 15 mL of deionized (DI) water to form an initial composite. By treating the PET NF surface with NaOH, the NF surface became more hydrophilic, allowing for the coating of MWCNTs in an aqueous solution [51,52]. The mixture was stirred for 30 min until homogeneous at room temperature. In the next step, the treated PET NF was thoroughly washed with deionized (DI) water many times before being allowed to dry at room temperature for 24 h. In the following step, the dried NF was soaked in an aqueous solution containing 0.02 g MWCNTs and 3.0 mL of deionized (DI) water in a glass petri dish (Ø18 cm) and allowed for drying at room temperature for 48 h before being used.

2.3. Methylene Blue Adsorption Batch Studies

The MB dye adsorption performance was optimized by adjusting the contact time, MB dye concentration, and PET NF-MWCNT dose. The pH of the mixture was adjusted after 3.0 mL of MB dye solution was mixed with a weighed sample of PET NF-MWCNTs composite. Before centrifugation, the mixture was agitated at 150 rpm for a set time at a constant temperature. When the spectra were taken using a spectrophotometer (JENEWAY-7315 Spectrophotometer, Staffordshire, United Kingdom), it was possible to determine how much MB dye was present in the supernatant.

The adsorption capacity (q) at equilibrium and time were calculated using Equations (1) and (2), while the dye removal percentage (R%) was calculated using Equation (3) [25,53,54]:

$$q_e = \frac{(C_i - C_e) \times V}{m} \quad (1)$$

$$q_t = \frac{(C_i - C_t) \times V}{m} \quad (2)$$

$$R\% = \frac{C_i - C_e}{C_i} \times 100 \quad (3)$$

where C_i is MB dye initial concentration (mg L^{-1}), C_e is MB equilibrium concentration (mg L^{-1}), C_t is MB concentration at time (mg L^{-1}), V is solution volume (L), and m is the mass of adsorbent (g).

2.4. Characterization of PET NF-MWCNTs Composite

The scanning electron microscope (SEM), Fourier transform infrared spectroscopy (FTIR), and X-ray diffraction (XRD) techniques were used to characterize the PET NF-MWCNTs composite that was synthesized in this study. The Quanta^{TM} 450 FEG was used to study the surface of the adsorbent material. The functional groups of the adsorbent were determined using a Shimadzu Prestige-21 spectrometric analyzer before and after MB adsorption. The X-ray diffractometer, Bruker-D8 Advance, was used to estimate the crystal structure of the composite across a 20–80° range (Cu-K_α radiation with λ = 1.54 Å). The pH measurements were carried out using a pHS-3C digital pH meter (made by Rex Instruments Factory in Shanghai, China).

2.5. Optimization of Adsorption Parameters

The Taguchi approach optimizes various operations while maintaining a cost-effective approach. Using orthogonal arrays (OA) enables the investigation of a large number of parameters with a limited number of tests [25,55]. The OA produces a set of well-balanced (minimal) experiments and the desired output in terms of optimal experimental circumstances, acts as an objective function for optimization, facilitates data interpretation, and predicts optimal results. Using Minitab 2019 (Minitab Inc., State College, PA, USA), an orthogonal L^{25} array with four tunable parameters (pH, initial MB dye concentration, adsorbent dose, and contact time) was selected. Each modifiable parameter was evaluated at five distinct levels, namely, L1, L2, L3, L4 and L5. The controllable parameters and their values used in the Taguchi design are summarized in Table 1 [56,57]. According to the arrangement shown in Table 1, a comprehensive factorial experimental design with four parameters and five levels per parameter would need 5^4 (625) experiments for this layout. The orthogonal array can reduce the number of experiments from 625 to 25, resulting in a considerable decrease in time and cost. It was decided to use the orthogonal array of L25 for this study because of its complexity and the available resources [58].

Table 1. Controllable parameters and their associated levels.

Parameter	Levels				
	1	**2**	**3**	**4**	**5**
pH	4	5	6	7	8
MB Initial concentration (mg L^{-1})	10	20	25	30	40
Adsorbent dose (g)	0.001	0.002	0.004	0.006	0.008
Contact time (min)	10	20	40	80	120

The Taguchi approach includes transforming the obtained experimental data into a signal-to-noise (S/N) ratio, which could then be used to assess the experiments' quality and the validity of the results. When the words "signal" and "noise" are used in conjunction

with an output characteristic, they refer to the desired value (mean) and the undesirable value (standard deviation), respectively. According to Equation (4), the data from the experiments is analyzed using the "Larger is Better" (LB) quality characteristic to figure out the best conditions and which factors are important in removing the MB dye [59–61].

$$S/N = -10 \log \left[\frac{1}{n} \sum_{i=1}^{n} \left(\frac{1}{y_i} \right)^2 \right] \quad (4)$$

n and y_i represent the repetition number and the experimental response.

2.6. Adsorption Isotherms and Kinetics Studies

To characterize the solid-liquid adsorption process, adsorption isotherms are essential, and they often provide critical information for boosting adsorbent efficiency. PET NF-MWCNTs composite adsorption behavior was investigated using two different adsorption isotherm models: Langmuir Equation (5) and Freundlich Equation (6). Their Equations are shown in the form [62,63], which is written as follows:

$$\frac{C_e}{q_e} = \left(\frac{1}{K_L \ Q_m} \right) + \frac{C_e}{Q_m} \quad (5)$$

$$\log q_e = \log K_F + \frac{1}{n} \log C_e \quad (6)$$

where Q_m is maximum adsorption capacity (mg g^{-1}), K_L is Langmuir constant (L mg^{-1}), K_F is Freundlich constant (L g^{-1}), and $\frac{1}{n}$ represents an empirical constant indicating the adsorption intensity.

Adsorption kinetics studies provide a great deal of relevant information on the mechanism and performance of adsorption that may be utilized to construct an industrial treatment facility. In this study, two kinetic models, pseudo-first-order Equation (7), and pseudo-second-order Equation (8), were used to model the experimental data and are stated as follows [53,64]:

$$\log (q_e - q_t) = \log q_e - \left(\frac{k_1}{2.303} \right) t \quad (7)$$

$$\frac{t}{q_t} = \frac{1}{k_2 \ q_e^2} + \frac{1}{q_e}(t) \quad (8)$$

where: k_1 is the pseudo-first-order model rate constant (min^{-1}), and k_2 is the pseudo-second-order model rate constant (g mg^{-1} min^{-1}).

3. Results and Discussion

3.1. Characterization of PET NF-MWCNTs Composite

Adsorption is a surface phenomenon whose effects are determined by the adsorbents' shape and porosity [65]. Figure 1a–d shows the morphological properties of PET NF, MWCNTs, and PET NF-MWCNTs composite before and after MB dye adsorption on the NF surface [64]. As shown in Figure 1a, the diameter of the electrospun PET NF was less than 100 nm. Figure 1b depicts a typical SEM image of MWCNTs. This view highlights the crystalline tubular structure of the nanotubes. It had an inner diameter of 5–10 nm, an outer diameter of 10–50 nm, and a length of 5–30 mm. Figure 1c depicts a PET NF-MWCNTs composite before MB dye adsorption. It shows the presence of MWCNTs on the surface of the PET NF and irregular pores of various shapes and sizes.

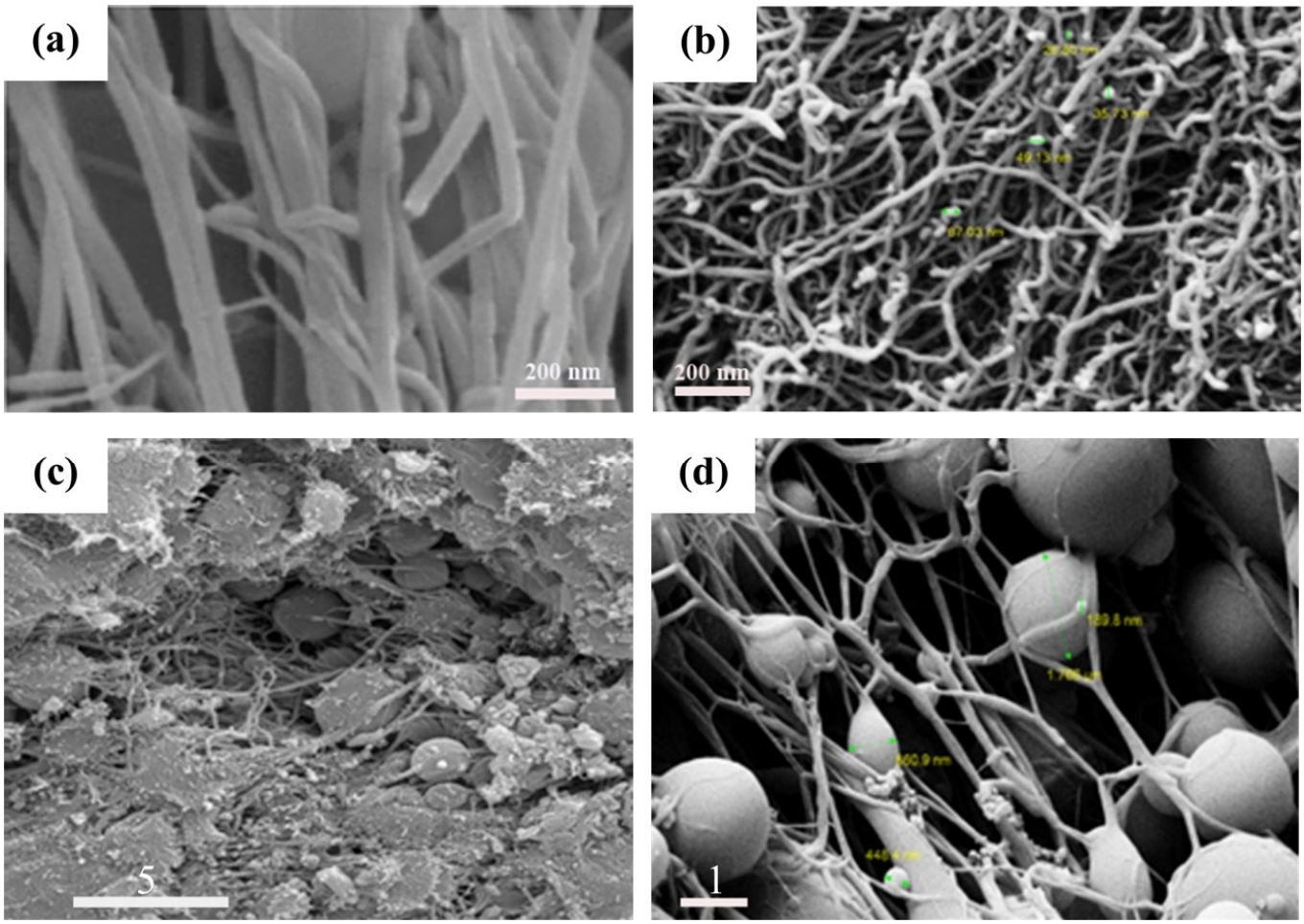

Figure 1. SEM images of the (**a**) PET NF, (**b**) MWCNTs, and PET NF-MWCNTs composite (**c**) before and (**d**) after adsorption of MB dye.

Interestingly, the surface was modified after the adsorption process, and the pores were filled with MB dye molecules, as in Figure 1d. In addition, the shape of beads may be related to the high feed rate and concentration of PET polymer solution compared to MWCNTs, which leads to defeating the surface tension by electrostatic forces periodically and incomplete drawing of the electrospun jet between the distance of the needle tip and collector. It was primarily responsible for the formation of bead-like structures rather than completely NFs [66,67].

Various functional groups on the PET NF-MWCNTs composite were investigated via FTIR spectroscopy. Compared to the FTIR for PET NF synthesized in the previous study [68], the addition of MWCNTs to the PET NF introduced some additional absorption bands to the spectra. Figure 2 depicts the unique peaks of the PET NF-MWCNTs composite adsorbent. The 2954 cm^{-1} band was assigned to the stretching vibrational of C–H aromatic and aliphatic groups. Carbonyl stretching (C=O) is responsible for the band at 1716 cm^{-1} [68]. The major peaks were detected at 1504 and 1400 cm^{-1} due to stretching vibrations of C=C and aromatic rings stretching, respectively [49]. CO–O stretching can be assigned to the band at 1246 cm^{-1}.

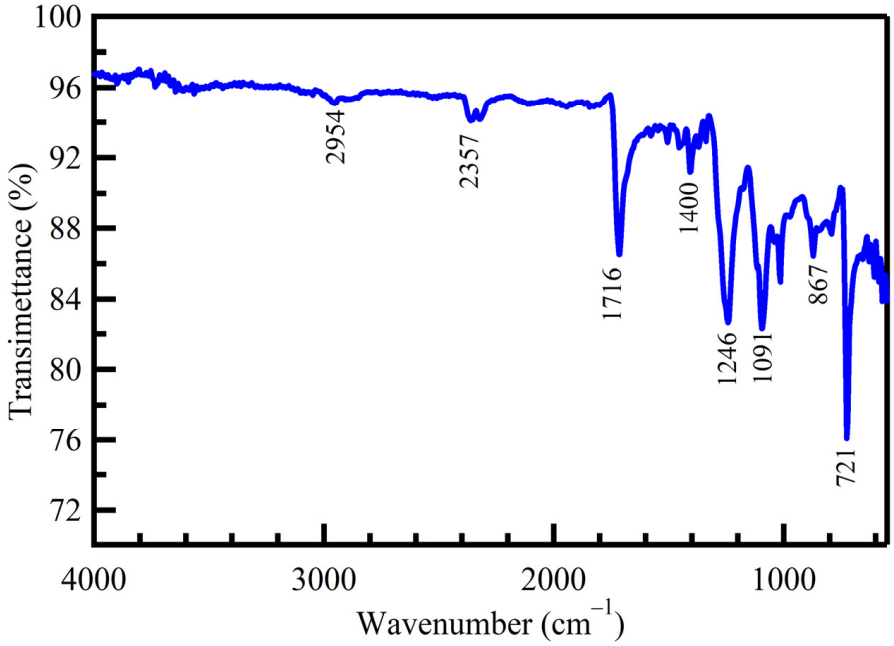

Figure 2. FTIR Spectra of PET NF-MWCNTs composite.

Furthermore, the peak at 1091 cm^{-1} was associated with gauche stretching vibrations of C-O. The distinctive peak at 721 cm^{-1} represents the presence of aromatic hydrocarbons. The PET NF-MWCNTs composite is combined with MB dye molecules, which have functional groups forming chemical bonds. The FTIR spectrum confirmed that the synthesized PET NF-MWCNTs had many oxygen functional groups. These groups can behave as accessible adsorption sites and contribute significantly to the MB dye removal process.

Figure 3 depicts XRD analysis of MWCNTs, and the PET NF-MWCNTs composite. The C (002) diffraction peak in the MWCNTs pattern at 2θ = 26.1° relates to an orderly arrangement of hexagonal graphitic cylinders. Graphite's C (100), C (004), and C (110) diffraction peaks at 2θ = 42.0°, 49.0°, and 72.5°, respectively, are also well-known [69]. The C (002) peak is absent from the PET NF-MWCNTs composite's XRD pattern. However, the XRD pattern of the PET NF-MWCNT composite exhibits an increase in the diffraction peaks at 42.0° and 49.0°, which are associated with PET NF. This is related to the PET polymer's progressive perfection and the well-established nucleating influence in the presence of MWCNTs, which dramatically speeds up the crystallization of PET NF [70].

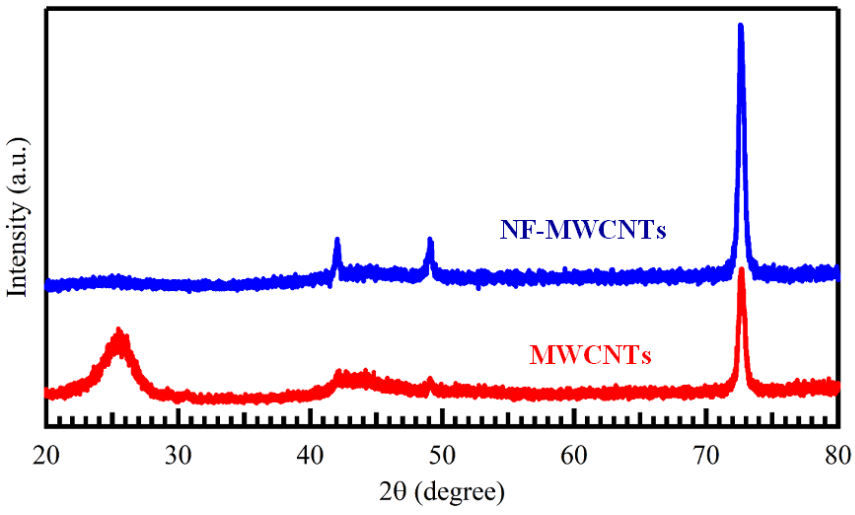

Figure 3. XRD patterns of MWCNTs and PET NF-MWCNTs composite.

3.2. Taguchi Optimization

3.2.1. Analysis of Experimental Data

The Taguchi approach determined the optimal conditions for MB dye adsorption by simultaneously varying four parameters at five levels. Table 2 displays the L25 (OA) and the findings collected after each of the four runs. Removal efficiency (R, %) was chosen as the response variable for the test. Depending on the modifiable parameters, between 19.67% and 99.49% of the MB dye could be removed [59,71].

Table 2. L25 Experimental design and expected results from Taguchi's (OA) analysis.

Run	pH	Conc. (mg L^{-1})	Dose (g)	Time (min)	Removal (%)	S/N Ratio
1	4	10	0.001	10	19.66	25.87
2	4	20	0.002	20	31.85	30.06
3	4	25	0.004	40	31.72	30.03
4	4	30	0.006	80	34.09	30.65
5	4	40	0.008	120	51.51	34.24
6	5	10	0.002	40	29.92	29.52
7	5	20	0.004	80	74.36	37.43
8	5	25	0.006	120	49.22	33.84
9	5	30	0.008	10	46.59	33.37
10	5	40	0.001	20	31.48	29.96
11	6	10	0.004	120	91.57	39.23
12	6	20	0.006	10	83.96	38.48
13	6	25	0.008	20	93.09	39.38
14	6	30	0.001	40	86.33	38.72
15	6	40	0.002	80	32.08	30.13
16	7	10	0.006	20	83.93	38.48
17	7	20	0.008	40	89.26	39.01
18	7	25	0.001	80	61.39	35.76
19	7	30	0.002	120	59.51	35.49
20	7	40	0.004	10	60.94	35.70
21	8	10	0.008	80	99.49	39.96
22	8	20	0.001	120	96.75	39.71
23	8	25	0.002	10	97.04	39.74
24	8	30	0.004	20	97.53	39.78
25	8	40	0.006	40	97.15	39.75

The S/N ratio is depicted in Figure 4 as the dependent parameters concerning pH, adsorbent dose, and contact time, as demonstrated in the main effect plot of MB dye removal percentage. Based on the figure, it is possible to identify the most important parameters and the optimum levels [72]. As a result, the optimal parameter levels for maximal %R of MB dye were pH of 8, 20 mg L^{-1} (MB dye initial concentration), the PET NF-MWCNTs dose of 0.008 g, and contact time of 120 min. Accordingly, the highest experimental MB dye removal effectiveness of 94.786% (S/N = 44.3068) was attained to verify that the anticipated response value was accurate and carried out under the above-mentioned optimal circumstances.

For each parameter level, the average of each response characteristic (S/N ratios) is presented in Table 3. The table is prioritized based on Delta values according to how much each parameter influences the others. Throughout the process, the pH of the solution was the most important parameter to consider. Next, the adsorbent dose is considered, followed by the MB dye concentration, with the contact time parameter having the least effect. PH values in the range of 4–8 reveal an improvement in dye removal efficacy as pH levels rise. In addition, the table optimizes the adsorption conditions. The adsorbent surface is positively charged. However, when pH values climb, the adsorbent surface becomes negatively charged, promoting electrostatic interaction with MB cations and, consequently, increasing efficiency. Because of the adsorption surface area of the adsorbent, the adsorbent dose affected the process efficiency by increasing the number of sites accessible for adsorption as the adsorbent dose was increased [25,73].

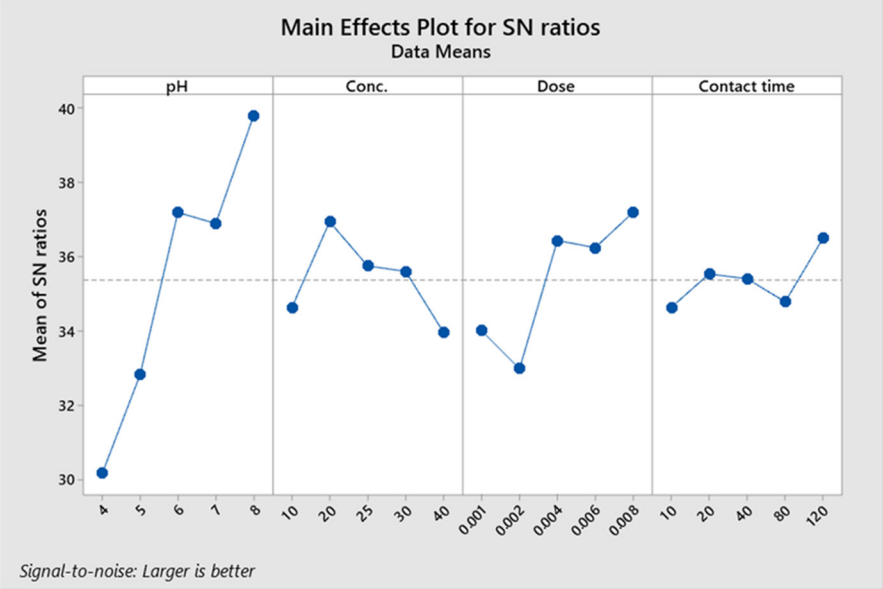

Figure 4. The S/N ratio of MB dye removal against pH, MB dye initial concentration, PET NF-MWCNTs dose, and contact time.

Table 3. The response of S/N ratios for the removal of MB dye.

Level	pH	Conc. (mg L^{-1})	Dose (g)	Time (min)
1	30.17	34.61	34.01	34.63
2	32.82	36.94 *	32.99	35.53
3	37.19	35.75	36.43	35.41
4	36.89	35.60	36.24	34.78
5	39.79 *	33.95	37.19 *	36.50 *
Delta	9.62	2.99	4.20	1.87
Rank	1	3	2	4

* The maximal signal-to-noise ratio (S/N) represents the optimal condition.

3.2.2. Analysis of Variance ANOVA

An Analysis of Variance (ANOVA) evaluated the overall relevance of different factors on the experiment response (%R). Table 4 displays the ANOVA findings. The values of freedom degree (DOF), the total sum of squares variance (SS), mean square (MS), Fisher's test (F-value), probability of occurrence (*p*-value), and percent of contribution (P, %) for each parameter in the response are obtained in ANOVA analysis (general linear model) [74]. According to the ANOVA design, the lower the *p*-value of the tested parameter (near to zero), the more successful it is. The sum of squares (SS) will be crucial under the same scenario, so the greater the SS value, the more effective [75]. The %P contributions of pH, initial MB dye concentration, adsorbent dose, and contact time were 71.01%, 5.91%, 12.08% and 1.81%, respectively. The pH solution had the greatest %P, indicating that the pH of the dye solution heavily impacted the adsorption process. However, the contact time had the lowest %P. Figure 5 graphically depicts the contribution of each parameter to MB dye adsorption. As can be observed, the results of the ANOVA analysis for MB dye adsorption from solution by the PET NF-MWCNTs composite were similar to the results of the preceding section's examination of the influence of the parameters studied.

3.3. Adsorption Isotherm Models

Isotherm investigations can explain how an adsorbate interacts with an adsorbent. When both phases are in equilibrium, the isotherm directs the dye concentration in solution and the quantity of dye adsorbed on the solid phase. While the Langmuir isotherm assumes monolayer adsorption on a homogeneous surface, the Freundlich isotherm addresses

multilayer adsorption on a heterogeneous surface with varied affinity. The linear forms of these models were used to investigate the interactions of MB dye on the surface of the PET NF-MWCNTs composite, as illustrated in Figure 6 [25,62,76]. Table 5 shows the derived values for the constants in the Langmuir and Freundlich equations and the regression correlation (R^2). It proves that the proposed findings for the adsorption of MB by the PET NF-MWCNTs composite match the Langmuir isotherm model owing to the high R^2 = 0.9997. This value demonstrates that the parameters are in consonance and validates the monolayer adsorption of MB onto the PET NF-MWCNTs composite. To sum up, the surface of the PET NF-MWCNTs composite was covered with the MB dye monolayer by an adsorption mechanism [77].

Table 4. Analysis of variance for the transformed response of % removal data.

Parameters	DOF	SS	MS	F-Value	*p*-Value	Contribution %P
pH	4	12,883.6	3220.91	15.44	0.001	71.01%
Concentration	4	1071.5	267.88	1.28	0.353	5.91%
Dose	4	2191.4	547.84	2.63	0.114	12.08%
Contact time	4	328.4	82.1	0.39	0.808	1.81%
Error	8	1669.2	208.66			9.20%
Total	24	18,144.2				100.00%

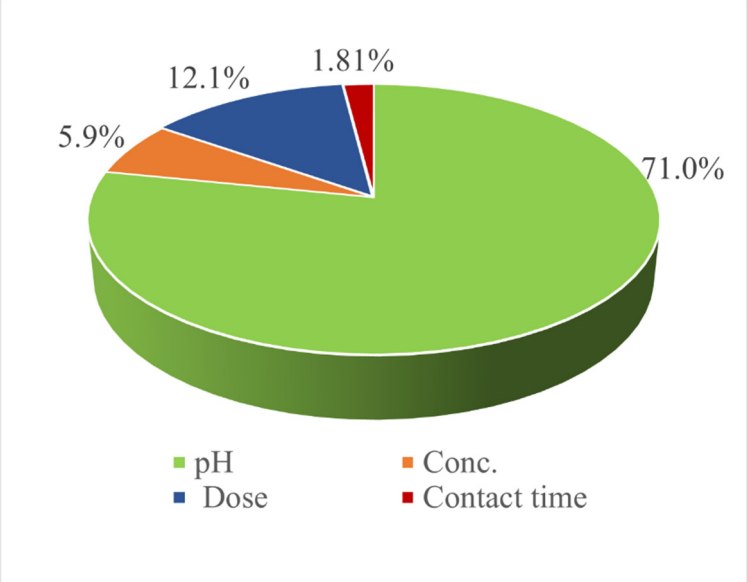

Figure 5. Percent of the contribution of various parameters.

In the Langmuir isotherm model, the value of Q_m = 7.047 mg g^{-1} reflects the quantity of MB dye required per unit weight of sorbent to create a complete monolayer on the surface of a PET NF-MWCNTs composite surface. As shown in Table 6, the adsorption capacity of the PET NF-MWCNTs composite for the adsorption of MB dye is compared to that of other adsorbents was made in previous studies. PET NF-MWCNTs composite adsorbs MB dye nicely, despite its lesser capacity than specific other adsorbents, which is considered an intermediate adsorbent compared to others. Furthermore, the adsorption is chemical, physical, and linear whether the value of n is less than one, more than one, or equal to one, respectively [72]. Because the value of n for the PET NF-MWCNTs composite is more than one, the dominant adsorption is physical adsorption [78] rather than chemical. In addition, $\frac{1}{n}$ value (0.821) is in the range $0 < \frac{1}{n} < 1$, therefore, the adsorption process is favorable [79].

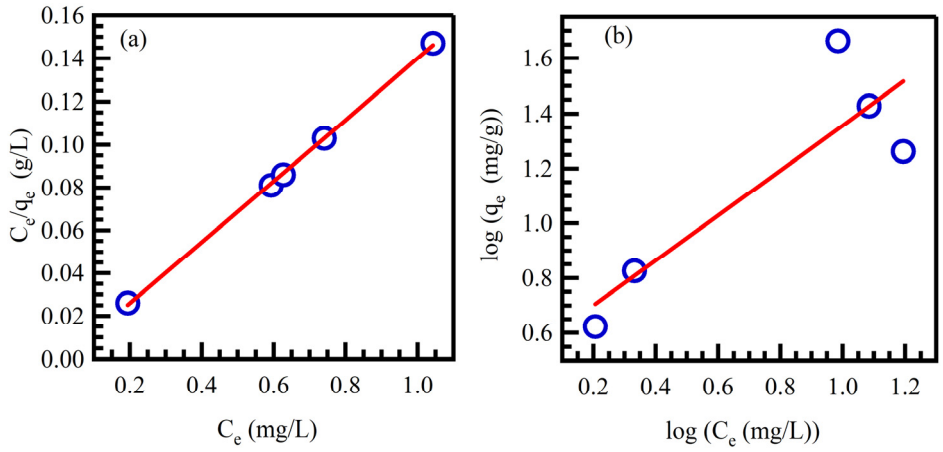

Figure 6. (**a**) Langmuir and (**b**) Freundlich adsorption isotherms for adsorption of MB dye.

Table 5. Langmuir and Freundlich isotherms parameters for MB adsorption by PET NF-MWCNTs composite.

Langmuir Parameters			Freundlich Parameters		
K_L (L mg^{-1})	Q_m (mg g^{-1})	R^2	K_F (L g^{-1})	n	R^2
67.571	7.047	0.9997	3.436	1.218	0.7645

Table 6. An overview of several adsorbents' adsorption capacities and conditions for removing MB dye.

Adsorbent Material	Q_m (mg g^{-1})	Time	pH	[Ref.]
OMWCNT– κ-carrageenan–Fe_3O_4	1.240	60 min	6.5	[80]
Phosphoric acid based geopolymers	3.010	90 min	10.0	[81]
Biochar derived from mixed municipal discarded material	5.018	6 h	5.0	[82]
Fly ash	5.718	60 min	8.0	[83]
Yellow passion fruit peel	6.800	56 h	9.0	[84]
PET NF-MWCNTs	7.047	120 min	8.0	This study
GPS/AA-MWCNTs NCs	10.300	-	4.0	[85]
PVA/VC-MWCNTs	16.844	45 min	12.0	[86]
N-maleyl chitosan/P (AA-co-VPA)	50.180	240 min	7.0	[87]
Garlic peel	82.640	210 min	6.0	[88]
Magnetized *Tectona grandis* sawdust	172.410	60 min	8.0	[89]

3.4. Adsorption Kinetic Models

To fully understand the characteristics of the adsorption process of the PET NF-MWCNTs composite and analyze the MB dye adsorption kinetics under optimal adsorption conditions (pH = 8, initial MB concentration is 20 mg L^{-1}, adsorbent dose of 0.008 g, and contact time of 120 min), the pseudo-first-order and pseudo-second-order kinetic models [29,90] were used to fit experimental data obtained from batch experiments (Figure 7). The kinetic parameters for each of these models are summarized in Table 7. The R^2 was determined to verify the validity of the models used. The pseudo-second-order kinetic model has substantially higher R^2 values than the pseudo-first-order kinetic model, demonstrating that the kinetics of MB dye adsorption follows the pseudo-second-order kinetic model. The calculated $(q_e)_{cal.}$ value for the pseudo-second-order kinetic model was quite compatible with the experimental $(q_e)_{exp.}$ value [65], showing that the model is correct. The pseudo-first-order kinetic model was used to study the adsorption of reversible systems, with equilibrium being achieved between the adsorbate and adsorbent systems. Consequently, the pseudo-second-order kinetic model outperforms the first-order model describing how the PET NF-MWCNTs composite removes MB dye from an aqueous solution.

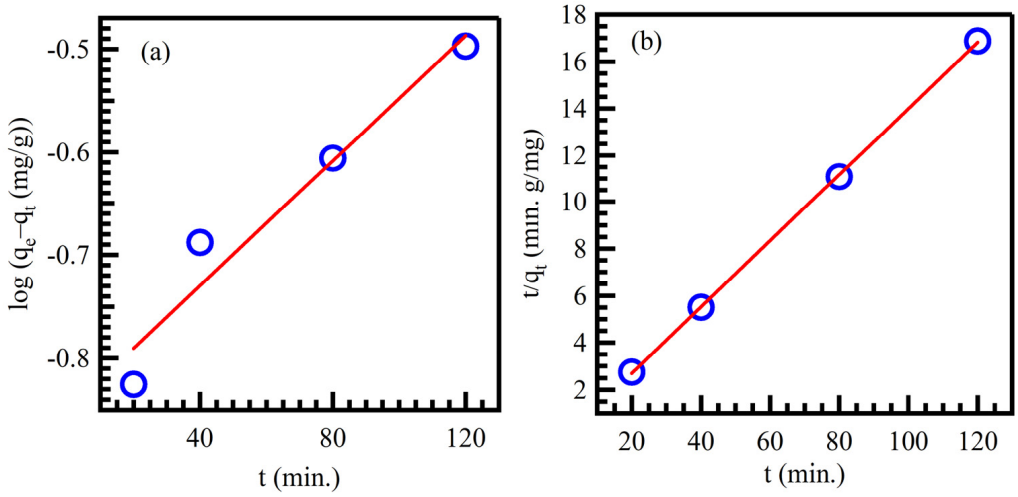

Figure 7. (**a**) The pseudo-first-order kinetic plot and (**b**) pseudo-second-order kinetic plot for MB dye adsorption.

Table 7. The kinetics parameters of the pseudo-first-order and pseudo-second-order for MB dye adsorption.

Pseudo First-Order Paramters				Pseudo Second-Order Paramters				
K_1 (min^{-1})	$(q_e)_{exp.}$ (mg g^{-1})	$(q_e)_{cal.}$ (mg g^{-1})	R^2	K_2 (g mg^{-1} min^{-1})	$(q_e)_{cal.}$ (mg g^{-1})	$(q_e)_{exp.}$ (mg g^{-1})	R^2	h
0.0069	7.427	0.1408	0.9467	0.2038	7.427	7.0972	0.9999	10.2669

4. Conclusions

The current work demonstrates that the PET NF-MWCNTs composite was effectively fabricated and exploited as an adsorbent to remove the MB dye from an aqueous solution. To find the optimal conditions, the Taguchi approach was used. It was concluded that the pH of the solution is the most important parameter in the adsorption process. The Langmuir isotherm describes the adsorption process and a pseudo-second-order kinetic model. According to the Langmuir isotherm model, the maximum adsorption capacity of the PET NF-MWCNTs composite was determined to be 7.047 mg g^{-1}. The PET NF-MWCNTS composite is expected to attract considerable attention as an effective adsorbent for many separation processes. The Taguchi approach will reduce experimental time by using many parameters with small experiments and economic viability.

Author Contributions: Conceptualization, S.A.Y., I.A.S. and G.A.M.A.; methodology, W.K.E., S.A.Y. and A.H.A.; software, W.K.E., I.A.S.; validation, A.H.A. and W.K.E.; formal analysis, S.A.Y., M.R.T. and G.A.M.A.; investigation, S.A.Y., K.F.C. and G.A.M.A.; resources, S.A.Y., I.A.S., W.K.E. and A.H.A.; data curation, G.A.M.A. and S.A.Y.; writing—original draft preparation, W.K.E. and A.H.A.; writing—review and editing, M.R.T., S.A.Y., K.F.C., M.A.A. and G.A.M.A.; visualization, S.A.Y. and G.A.M.A.; supervision, S.A.Y., I.A.S. and G.A.M.A.; project administration, S.A.Y., M.A.A., K.F.C. and G.A.M.A.; funding acquisition, S.A.Y. and M.A.A. All authors have read and agreed to the published version of the manuscript.

Funding: This research received no external funding.

Institutional Review Board Statement: Not applicable.

Informed Consent Statement: Not applicable.

Data Availability Statement: The data presented in this study are available in the article.

Acknowledgments: S.A.Y. is grateful for the financial support by USAID Partnerships for Enhanced Engagement in Research (PEER) Program—an international grants program that funds scientists and engineers in developing countries who partner with U.S. government-funded researchers to address global development challenges. The U.S. National Academies of Sciences administered Engineering and Medicine (NASEM), PEER/Iraq project/cycle 6. In addition, M.A.A. extends his appreciation to the Deanship of Scientific Research at King Khalid University for funding this work through the research group project under grant number (KKU/RCAMS/G015-21). S.A.Y. thanks Mohammed AbdulHakim Alsaadi, National Chair of Materials Science and Metallurgy, University of Nizwa, Oman, for the research support.

Conflicts of Interest: The authors declare no conflict of interest.

References

1. Bolisetty, S.; Peydayesh, M.; Mezzenga, R. Sustainable technologies for water purification from heavy metals: Review and analysis. *Chem. Soc. Rev.* **2019**, *48*, 463–487. [CrossRef] [PubMed]
2. Bayomie, O.S.; Kandeel, H.; Shoeib, T.; Yang, H.; Youssef, N.; El-Sayed, M.M.H. Novel approach for effective removal of methylene blue dye from water using fava bean peel waste. *Sci. Rep.* **2020**, *10*, 7824. [CrossRef] [PubMed]
3. Viscusi, G.; Lamberti, E.; Gorrasi, G. Design of a hybrid bio-adsorbent based on Sodium Alginate/Halloysite/Hemp hurd for methylene blue dye removal: Kinetic studies and mathematical modeling. *Colloids Surf. A Physicochem. Eng. Asp.* **2022**, *633*, 127925. [CrossRef]
4. Besharati, N.; Alizadeh, N.; Shariati, S. Removal of cationic dye methylene blue (Mb) from aqueous solution by coffee and peanut husk modified with magnetite iron oxide nanoparticles. *J. Mex. Chem. Soc.* **2018**, *62*, 110–124. [CrossRef]
5. Robati, D.; Mirza, B.; Ghazisaeidi, R.; Rajabi, M.; Moradi, O.; Tyagi, I.; Agarwal, S.; Gupta, V.K. Adsorption behavior of methylene blue dye on nanocomposite multi-walled carbon nanotube functionalized thiol (MWCNT-SH) as new adsorbent. *J. Mol. Liq.* **2016**, *216*, 830–835. [CrossRef]
6. Hor, K.Y.; Chee, J.M.C.; Chong, M.N.; Jin, B.; Saint, C.; Poh, P.E.; Aryal, R. Evaluation of physicochemical methods in enhancing the adsorption performance of natural zeolite as low-cost adsorbent of methylene blue dye from wastewater. *J. Clean. Prod.* **2016**, *118*, 197–209. [CrossRef]
7. Cheng, J.; Zhan, C.; Wu, J.; Cui, Z.; Si, J.; Wang, Q.; Peng, X.; Turng, L.S. Highly Efficient Removal of Methylene Blue Dye from an Aqueous Solution Using Cellulose Acetate Nanofibrous Membranes Modified by Polydopamine. *ACS Omega* **2020**, *5*, 5389–5400. [CrossRef]
8. Yasin, S.A.; Abbas, J.A.; Saeed, I.A.; Ahmed, I.H. The application of green synthesis of metal oxide nanoparticles embedded in polyethylene terephthalate nanofibers in the study of the photocatalytic degradation of methylene blue. *Polym. Bull.* **2020**, *77*, 3473–3484. [CrossRef]
9. Laouini, S.E.; Bouafia, A.; Soldatov, A.V.; Algarni, H.; Tedjani, M.L.; Ali, G.A.M.; Barhoum, A. Green Synthesized of Ag/Ag_2O Nanoparticles Using Aqueous Leaves Extracts of Phoenix dactylifera L. and Their Azo Dye Photodegradation. *Membranes* **2021**, *11*, 468. [CrossRef]
10. Ethiraj, A.S.; Rhen, D.S.; Soldatov, A.V.; Ali, G.A.M.; Bakr, Z.H. Efficient and recyclable Cu incorporated TiO_2 nanoparticle catalyst for organic dye photodegradation. *Int. J. Thin Film. Sci. Technol.* **2021**, *10*, 169–182.
11. Sharifi, A.; Montazerghaem, L.; Naeimi, A.; Abhari, A.R.; Vafaee, M.; Ali, G.A.M.; Sadegh, H. Investigation of photocatalytic behavior of modified ZnS:Mn/MWCNTs nanocomposite for organic pollutants effective photodegradation. *J. Environ. Manag.* **2019**, *247*, 624–632. [CrossRef]
12. Naeimi, A.; Sharifi, A.; Montazerghaem, L.; Abhari, A.R.; Mahmoodi, Z.; Bakr, Z.H.; Soldatov, A.V.; Ali, G.A.M. Transition metals doped WO_3 photocatalyst towards high efficiency decolourization of azo dye. *J. Mol. Struct.* **2022**, *1250*, 131800. [CrossRef]
13. Son, G.; Lee, H. Methylene blue removal by submerged plasma irradiation system in the presence of persulfate. *Environ. Sci. Pollut. Res.* **2016**, *23*, 15651–15656. [CrossRef]
14. Selim, M.T.; Salem, S.S.; Mohamed, A.A.; El-Gamal, M.S.; Awad, M.F.; Fouda, A. Biological treatment of real textile effluent using aspergillus flavus and fusarium oxysporium and their consortium along with the evaluation of their phytotoxicity. *J. Fungi* **2021**, *7*, 193. [CrossRef]
15. Alhasan, H.S.; Alahmadi, N.; Yasin, S.A.; Khalaf, M.Y.; Ali, G.A.M. Low-Cost and Eco-Friendly Hydroxyapatite Nanoparticles Derived from Eggshell Waste for Cephalexin Removal. *Separations* **2022**, *9*, 10. [CrossRef]
16. Mahmoodi, Z.; Abhari, A.R.; Lalehloo, R.S.; Bakr, Z.H.; Ali, G.A.M. Thermodynamic Studies on the Adsorption of Organophosphate Pesticides (Diazinon) onto ZnO/Polyethersulfone Nanocomposites. *ChemistrySelect* **2022**, *7*, e202103619. [CrossRef]
17. Sadegh, H.; Ali, G.A.M.; Nia, H.J.; Mahmoodi, Z. Nanomaterial surface modifications for enhancement of the pollutant adsorption from wastewater: Adsorption of nanomaterials. In *Nanotechnology Applications in Environmental Engineering*; IGI Global: Hershey, PA, USA, 2019. [CrossRef]
18. Sadegh, H.; Ali, G.A.M.; Makhlouf, A.S.H.; Chong, K.F.; Alharbi, N.S.; Agarwal, S.; Gupta, V.K. MWCNTs-Fe_3O_4 nanocomposite for Hg (II) high adsorption efficiency. *J. Mol. Liq.* **2018**, *258*, 345–353. [CrossRef]

19. Habeeb, O.A.; Ramesh, K.; Ali, G.A.M.; Yunus, R.M. Low-cost and eco-friendly activated carbon from modified palm kernel shell for hydrogen sulfide removal from wastewater: Adsorption and kinetic studies. *Desalination Water Treat.* **2017**, *84*, 205–214. [CrossRef]
20. Asfaram, A.; Ghaedi, M.; Hajati, S.; Goudarzi, A. Synthesis of magnetic γ-Fe2O3-based nanomaterial for ultrasonic assisted dyes adsorption: Modeling and optimization. *Ultrason. Sonochem.* **2016**, *32*, 418–431. [CrossRef]
21. Sadegh, H.; Ali, G.A.M.; Abbasi, Z.; Nadagoud, M.N. Adsorption of Ammonium Ions onto Multi-Walled Carbon Nanotubes. *Studia Univ. Babes-Bolyai Chem.* **2017**, *62*, 233–245. [CrossRef]
22. Habeeb, O.A.; Ramesh, K.; Ali, G.A.M.; Yunus, R.M. Isothermal modelling based experimental study of dissolved hydrogen sulfide adsorption from wastewater using eggshell based activated carbon. *Malays. J. Anal. Sci.* **2017**, *21*, 334–345.
23. Abdel Ghafar, H.H.; Ali, G.A.M.; Fouad, O.A.; Makhlouf, S.A. Enhancement of adsorption efficiency of methylene blue on Co_3O_4/SiO_2 nanocomposite. *Desalination Water Treat.* **2015**, *53*, 2980–2989. [CrossRef]
24. Tebyetekerwa, M.; Xu, Z.; Yang, S.; Ramakrishna, S. Electrospun nanofibers-based face masks. *Adv. Fiber Mater.* **2020**, *2*, 161–166. [CrossRef]
25. Mosoarca, G.; Popa, S.; Vancea, C.; Boran, S. Optimization, equilibrium and kinetic modeling of methylene blue removal from aqueous solutions using dry bean pods husks powder. *Materials* **2021**, *14*, 5673. [CrossRef]
26. Adil, H.I.; Thalji, M.R.; Yasin, S.A.; Saeed, I.A.; Assiri, M.A.; Chong, K.F.; Ali, G.A.M. Metal–organic frameworks (MOFs) based nanofiber architectures for the removal of heavy metal ions. *RSC Adv.* **2022**, *12*, 1433–1450. [CrossRef]
27. Xiao, S.; Shen, M.; Guo, R.; Huang, Q.; Wang, S.; Shi, X. Fabrication of multiwalled carbon nanotube-reinforced electrospun polymer nanofibers containing zero-valent iron nanoparticles for environmental applications. *J. Mater. Chem.* **2010**, *20*, 5700–5708. [CrossRef]
28. Ibupoto, A.S.; Qureshi, U.A.; Ahmed, F.; Khatri, Z.; Khatri, M.; Maqsood, M.; Brohi, R.Z.; Kim, I.S. Reusable carbon nanofibers for efficient removal of methylene blue from aqueous solution. *Chem. Eng. Res. Des.* **2018**, *136*, 744–752. [CrossRef]
29. Shabaan, O.A.; Jahin, H.S.; Mohamed, G.G. Removal of anionic and cationic dyes from wastewater by adsorption using multiwall carbon nanotubes. *Arab. J. Chem.* **2020**, *13*, 4797–4810. [CrossRef]
30. Xu, J.; Cao, Z.; Zhang, Y.; Yuan, Z.; Lou, Z.; Xu, X.; Wang, X. A review of functionalized carbon nanotubes and graphene for heavy metal adsorption from water: Preparation, application, and mechanism. *Chemosphere* **2018**, *195*, 351–364. [CrossRef]
31. May-Pat, A.; Avilés, F.; Toro, P.; Yazdani-Pedram, M.; Cauich-Rodríguez, J.V. Mechanical properties of PET composites using multiwalled carbon nanotubes functionalized by inorganic and itaconic acids. *Express Polym. Lett.* **2012**, *6*, 96–106. [CrossRef]
32. Aryaei, A.; Jayatissa, A.H.; Jayasuriya, A.C. Mechanical and biological properties of chitosan/carbon nanotube nanocomposite films. *J. Biomed. Mater. Res. Part A* **2014**, *102*, 2704–2712. [CrossRef] [PubMed]
33. Saifuddin, N.; Raziah, A.Z.; Junizah, A.R. Carbon nanotubes: A review on structure and their interaction with proteins. *J. Chem.* **2013**, *2013*, 676815. [CrossRef]
34. Hu, M.; Zhao, Z.; Tian, F.; Oganov, A.R.; Wang, Q.; Xiong, M.; Fan, C.; Wen, B.; He, J.; Yu, D.; et al. Compressed carbon nanotubes: A family of new multifunctional carbon allotropes. *Sci. Rep.* **2013**, *3*, 1331. [CrossRef] [PubMed]
35. Ali, G.A.M.; Megiel, E.; Cieciórski, P.; Thalji, M.R.; Romański, J.; Algarni, H.; Chong, K.F. Ferrocene functionalized multi-walled carbon nanotubes as supercapacitor electrodes. *J. Mol. Liq.* **2020**, *318*, 114064. [CrossRef]
36. Ganesh, E.N. Single Walled and Multi Walled Carbon Nanotube Structure. *Synthesis Appl.* **2013**, *2*, 311–320.
37. Tlili, I.; Alkanhal, T.A. Nanotechnology for water purification: Electrospun nanofibrous membrane in water and wastewater treatment. *J. Water Reuse Desalin.* **2019**, *9*, 232–247. [CrossRef]
38. Cui, J.; Li, F.; Wang, Y.; Zhang, Q.; Ma, W.; Huang, C. Electrospun nanofiber membranes for wastewater treatment applications. *Sep. Purif. Technol.* **2020**, *250*, 117116. [CrossRef]
39. Essa, W.K.; Yasin, S.A.; Saeed, I.A.; Ali, G.A.M. Nanofiber-Based Face Masks and Respirators as COVID-19 Protection: A Review. *Membranes* **2021**, *11*, 250. [CrossRef]
40. Kugarajah, V.; Ojha, A.K.; Ranjan, S.; Dasgupta, N.; Ganesapillai, M.; Dharmalingam, S.; Elmoll, A.; Hosseini, S.A.; Muthulakshmi, L.; Vijayakumar, S.; et al. Future applications of electrospun nanofibers in pressure driven water treatment: A brief review and research update. *J. Environ. Chem. Eng.* **2021**, *9*, 105107. [CrossRef]
41. Thamer, B.M.; Aldalbahi, A.; Moydeen, A.M.; Rahaman, M.; El-Newehy, M.H. Modified Electrospun Polymeric Nanofibers and Their Nanocomposites as Nanoadsorbents for Toxic Dye Removal from Contaminated Waters: A Review. *Polymers* **2021**, *13*, 20. [CrossRef]
42. Liu, Z.; Wang, H.; Wang, E.; Zhang, X.; Yuan, R.; Zhu, Y. Superhydrophobic poly (vinylidene fluoride) membranes with controllable structure and tunable wettability prepared by one-step electrospinning. *Polymer* **2016**, *82*, 105–113. [CrossRef]
43. Najafi, M.; Frey, M.W. Electrospun nanofibers for chemical separation. *Nanomaterials* **2020**, *10*, 982. [CrossRef]
44. Altaleb, H.A.; Thamer, B.M.; Abdulhameed, M.M.; El-Hamshary, H.; Mohammady, S.Z.; Al-Enizi, A.M. Efficient electrospun terpolymer nanofibers for the removal of cationic dyes from polluted waters: A non-linear isotherm and kinetic study. *J. Environ. Chem. Eng.* **2021**, *9*, 105361. [CrossRef]
45. Thamer, B.M.; Aldalbahi, A.; Moydeen, A.M.; Al-Enizi, A.M.; El-Hamshary, H.; El-Newehy, M.H. Synthesis of aminated electrospun carbon nanofibers and their application in removal of cationic dye. *Mater. Res. Bull.* **2020**, *132*, 111003. [CrossRef]
46. Wang, H.; Chhowalla, M.; Sano, N.; Jia, S.; Amaratunga, G.A.J. Large-scale synthesis of single-walled carbon nanohorns by submerged arc. *Nanotechnology* **2004**, *15*, 546. [CrossRef]

47. Elliott, J.A.; Sandler, J.K.W.; Windle, A.H.; Young, R.J.; Shaffer, M.S.P. Collapse of single-wall carbon nanotubes is diameter dependent. *Phys. Rev. Lett.* **2004**, *92*, 95501. [CrossRef]
48. Thamer, B.M.; Aldalbahi, A.; Meera, M.A.; El-Newehy, M.H. In situ preparation of novel porous nanocomposite hydrogel as effective adsorbent for the removal of cationic dyes from polluted water. *Polymers* **2020**, *12*, 3002. [CrossRef]
49. Aljumaily, M.M.; Alsaadi, M.A.; Das, R.; Abd Hamid, S.B.; Hashim, N.A.; AlOmar, M.K.; Alayan, H.M.; Novikov, M.; Alsalhy, Q.F.; Hashim, M.A. Optimization of the synthesis of superhydrophobic carbon nanomaterials by chemical vapor deposition. *Sci. Rep.* **2018**, *8*, 2778. [CrossRef]
50. Ahmed, H.; Saleem, P.; Yasin, S.; Saeed, I. A Kinetic Study of Removing Methylene Blue from Aqueous Solutions by Modified Electrospun Polyethelene Terephthalate Nanofibres. *Egypt. J. Chem.* **2021**, *64*, 2803–2813.
51. Afonso, E.; Martínez-Gómez, A.; Huerta, A.; Tiemblo, P.; García, N. Facile Preparation of Hydrophobic PET Surfaces by Solvent Induced Crystallization. *Coatings* **2022**, *12*, 137. [CrossRef]
52. Tserengombo, B.; Jeong, H.; Dolgor, E.; Delgado, A.; Kim, S. Effects of Functionalization in Different Conditions and Ball Milling on the Dispersion and Thermal and Electrical Conductivity of MWCNTs in Aqueous Solution. *Nanomaterials* **2021**, *11*, 1323. [CrossRef]
53. Shayegan, H.; Ali, G.A.M.; Safarifard, V. Amide-Functionalized Metal–Organic Framework for High Efficiency and Fast Removal of Pb (II) from Aqueous Solution. *J. Inorg. Organomet. Polym. Mater.* **2020**, *30*, 3170–3178. [CrossRef]
54. Thamer, B.M.; Aldalbahi, A.; Moydeen, A.M.; El-Hamshary, H.; Al-Enizi, A.M.; El-Newehy, M.H. Effective adsorption of Coomassie brilliant blue dye using poly (phenylene diamine) grafted electrospun carbon nanofibers as a novel adsorbent. *Mater. Chem. Phys.* **2019**, *234*, 133–145. [CrossRef]
55. Taiwo, A.E.; Madzimbamuto, T.N.; Ojumu, T.V. Optimization of process variables for acetoin production in a bioreactor using Taguchi orthogonal array design. *Heliyon* **2020**, *6*, e05103. [CrossRef]
56. Korake, S.R.; Jadhao, P.D. Investigation of Taguchi optimization, equilibrium isotherms, and kinetic modeling for cadmium adsorption onto deposited silt. *Heliyon* **2021**, *7*, e05755. [CrossRef]
57. Gümüş, D.; Gümüş, F. Removal of Hydroxychloroquine Using Engineered Biochar from Algal Biodiesel Industry Waste: Characterization and Design of Experiment (DoE). *Arab. J. Sci. Eng.* **2021**. [CrossRef]
58. Newsha, J.; Abdolhadi, F. The thermodynamic and kinetics study of removal of cd(II) by nanoparticles of cobalt oxide in aqueous solution. *Iran. J. Chem. Chem. Eng.* **2019**, *38*, 127–139.
59. Ghosh, S.B.; Mondal, N.K. Application of Taguchi method for optimizing the process parameters for the removal of fluoride by Al-impregnated Eucalyptus bark ash. *Environ. Nanotechnol. Monit. Manag.* **2019**, *11*, 100206. [CrossRef]
60. Fernández-López, J.A.; Angosto, J.M.; Roca, M.J.; Doval Miñarro, M. Taguchi design-based enhancement of heavy metals bioremoval by agroindustrial waste biomass from artichoke. *Sci. Total Environ.* **2019**, *653*, 55–63. [CrossRef]
61. Asadi, F.; Asgari, G.; Seid-Mohammadi, A.; Torkshavand, Z. Optimization of hydrogen peroxide/nio nanoparticle photocatalytic process by degrading cephalexin from aqueous solution using taguchi method: Mineralization, mechanism and pathway. *Desalin. Water Treat.* **2020**, *201*, 323–337. [CrossRef]
62. Rojas, J.; Suarez, D.; Moreno, A.; Silva-Agredo, J.; Torres-Palma, R.A. Kinetics, isotherms and thermodynamic modeling of liquid phase adsorption of crystal violet dye onto shrimp-waste in its raw, pyrolyzed material and activated charcoals. *Appl. Sci.* **2019**, *9*, 5337. [CrossRef]
63. Alvarez-Torrellas, S.; Boutahala, M.; Boukhalfa, N.; Munoz, M. Effective adsorption of methylene blue dye onto magnetic nanocomposites. Modeling and reuse studies. *Appl. Sci.* **2019**, *9*, 4563. [CrossRef]
64. Yasin, S.A.; Zeebaree, S.Y.S.; Zeebaree, A.Y.S.; Zebari, O.I.H.; Saeed, I.A. The efficient removal of methylene blue dye using CuO/PET nanocomposite in Aqueous solutions. *Catalysts* **2021**, *11*, 241. [CrossRef]
65. Berkane, N.; Meziane, S.; Aziri, S. Optimization of Congo red removal from aqueous solution using Taguchi experimental design. *Sep. Sci. Technol.* **2020**, *55*, 278–288. [CrossRef]
66. Lee, K.H.; Kim, H.Y.; Bang, H.J.; Jung, Y.H.; Lee, S.G. The change of bead morphology formed on electrospun polystyrene fibers. *Polymer* **2003**, *44*, 4029–4034. [CrossRef]
67. Jafari, S.; Hosseini Salekdeh, S.S.; Solouk, A.; Yousefzadeh, M. Electrospun polyethylene terephthalate (PET) nanofibrous conduit for biomedical application. *Polym. Adv. Technol.* **2020**, *31*, 284–296. [CrossRef]
68. Abbas, J.A.; Said, I.A.; Mohamed, M.A.; Yasin, S.A.; Ali, Z.A.; Ahmed, I.H. Electrospinning of polyethylene terephthalate (PET) nanofibers: Optimization study using taguchi design of experiment. *IOP Conf. Ser. Mater. Sci. Eng.* **2018**, *454*, 12130. [CrossRef]
69. Alexiou, V.F.; Mathioudakis, G.N.; Andrikopoulos, K.S.; Beobide, A.S.; Voyiatzis, G.A. Poly(Ethylene terephthalate) carbon-based nanocomposites: A crystallization and molecular orientation study. *Polymers* **2020**, *12*, 2626. [CrossRef]
70. Mayoral, B.; Hornsby, P.R.; McNally, T.; Schiller, T.L.; Jack, K.; Martin, D.J. Quasi-solid state uniaxial and biaxial deformation of PET/MWCNT composites: Structural evolution, electrical and mechanical properties. *RSC Adv.* **2013**, *3*, 5162–5183. [CrossRef]
71. Madan, S.S.; Wasewar, K.L. Optimization for benzeneacetic acid removal from aqueous solution using CaO2 nanoparticles based on Taguchi method. *J. Appl. Res. Technol.* **2017**, *15*, 332–339. [CrossRef]
72. Yusuff, A.S.; Ajayi, O.A.; Popoola, L.T. Application of Taguchi design approach to parametric optimization of adsorption of crystal violet dye by activated carbon from poultry litter. *Sci. Afr.* **2021**, *13*, e00850. [CrossRef]
73. Pang, J.; Fu, F.; Ding, Z.; Lu, J.; Li, N.; Tang, B. Adsorption behaviors of methylene blue from aqueous solution on mesoporous birnessite. *J. Taiwan Inst. Chem. Eng.* **2017**, *77*, 168–176. [CrossRef]

74. Rezaei, H.; Haghshenasfard, M.; Moheb, A. Optimization of dye adsorption using Fe3O4 nanoparticles encapsulated with alginate beads by Taguchi method. *Adsorpt. Sci. Technol.* **2017**, *35*, 55–71. [CrossRef]
75. Kazemi, Z.; Ghiasi, R.; Jamehbozorgi, S. A theoretical study of the influence of solvent polarity on the structure and spectral properties in the interaction of C 20 and Si 2 H 2. *J. Nanoanal.* **2019**, *6*, 121–128.
76. Ai, L.; Zhang, C.; Liao, F.; Wang, Y.; Li, M.; Meng, L.; Jiang, J. Removal of methylene blue from aqueous solution with magnetite loaded multi-wall carbon nanotube: Kinetic, isotherm and mechanism analysis. *J. Hazard. Mater.* **2011**, *198*, 282–290. [CrossRef]
77. Goharrizi, A.S.; Azadi, M.; Shahryari, Z. Experimental study of methylene blue adsorption from aqueous solutions onto carbon nano tubes. *Int. J. Water Resour. Environ. Eng.* **2010**, *2*, 16–28.
78. Yildiz, D.; Keskin, F.; Demirak, A. Biosorption of 2,4 dichlorophenol onto Turkish Sweetgum bark in a batch system: Equilibrium and kinetic study. *Acta Chim. Slov.* **2017**, *64*, 237–247. [CrossRef]
79. Ragadhita, R.; Nandiyanto, A.B.D. How to calculate adsorption isotherms of particles using two-parameter monolayer adsorption models and equations. *Indones. J. Sci. Technol.* **2021**, *6*, 205–234. [CrossRef]
80. Duman, O.; Tunç, S.; Polat, T.G.; Bozoğlan, B.K.I. Synthesis of magnetic oxidized multiwalled carbon nanotube-κ-carrageenan-Fe3O4 nanocomposite adsorbent and its application in cationic Methylene Blue dye adsorption. *Carbohydr. Polym.* **2016**, *147*, 79–88. [CrossRef]
81. Khan, M.I.; Min, T.K.; Azizli, K.; Sufian, S.; Ullah, H.; Man, Z. Effective removal of methylene blue from water using phosphoric acid based geopolymers: Synthesis, characterizations and adsorption studies. *RSC Adv.* **2015**, *5*, 61410–61420. [CrossRef]
82. Hoslett, J.; Ghazal, H.; Mohamad, N.; Jouhara, H. Removal of methylene blue from aqueous solutions by biochar prepared from the pyrolysis of mixed municipal discarded material. *Sci. Total Environ.* **2020**, *714*, 136832. [CrossRef] [PubMed]
83. Kumar, K.V.; Ramamurthi, V.; Sivanesan, S. Modeling the mechanism involved during the sorption of methylene blue onto fly ash. *J. Colloid Interface Sci.* **2005**, *284*, 14–21. [CrossRef] [PubMed]
84. Pavan, F.A.; Mazzocato, A.C.; Gushikem, Y. Removal of methylene blue dye from aqueous solutions by adsorption using yellow passion fruit peel as adsorbent. *Bioresour. Technol.* **2008**, *99*, 3162–3165. [CrossRef] [PubMed]
85. Mallakpour, S.; Rashidimoghadam, S. Application of ultrasonic irradiation as a benign method for production of glycerol plasticized-starch/ascorbic acid functionalized MWCNTs nanocomposites: Investigation of methylene blue adsorption and electrical properties. *Ultrason. Sonochem.* **2018**, *40*, 419–432. [CrossRef]
86. Mallakpour, S.; Rashidimoghadam, S. Poly (vinyl alcohol)/Vitamin C-multi walled carbon nanotubes composites and their applications for removal of methylene blue: Advanced comparison between linear and nonlinear forms of adsorption isotherms and kinetics models. *Polymer* **2019**, *160*, 115–125. [CrossRef]
87. Nakhjiri, M.T.; Marandi, G.B.; Kurdtabar, M. Poly (AA-co-VPA) hydrogel cross-linked with N-maleyl chitosan as dye adsorbent: Isotherms, kinetics and thermodynamic investigation. *Int. J. Biol. Macromol.* **2018**, *117*, 152–166. [CrossRef]
88. Hameed, B.H.; Ahmad, A.A. Batch adsorption of methylene blue from aqueous solution by garlic peel, an agricultural waste biomass. *J. Hazard. Mater.* **2009**, *164*, 870–875. [CrossRef]
89. Mashkoor, F.; Nasar, A. Magnetized Tectona grandis sawdust as a novel adsorbent: Preparation, characterization, and utilization for the removal of methylene blue from aqueous solution. *Cellulose* **2020**, *27*, 2613–2635. [CrossRef]
90. Nizam, N.U.M.; Hanafiah, M.M.; Mahmoudi, E.; Halim, A.A.; Mohammad, A.W. The removal of anionic and cationic dyes from an aqueous solution using biomass-based activated carbon. *Sci. Rep.* **2021**, *11*, 1–17. [CrossRef]